Restoration of Anisoplanatic Astronomical Image by Using Blind Deconvolution

Luo Lin Wang Li

(*School of Physical Science and Technology, Southwest Jiaotong University, Chengdu, Sichuan* 610031, *China*)

* *Corresponding author*: *happyluolin@vip.163.com*

Abstract The point spread function of atmospheric turbulence is space variant where the field-of-view of the ground-based optical telescope is greater than the isoplanatic angle. The effects of anisoplanatism in image degrade the image quality recovered by conventional image processing based on the imaging technique of the space-invariant point spread function. An approach is to partition the ansioplanatic image into sub-region images corresponding to the isoplanatic angle. The sub-region images are then reconstructed by the conjugate gradient blind deconvolution algorithm. To avoid ringing at the edges, a window function is used to smooth the image edges. After each sub-image is restored, the full image is assembled by the seamless split and overlapping. The experimental results suggest that the proposed approach is effective to improve the restored image quality from the anisoplanatic image degraded by atmospheric turbulence.

OCIS codes 010.1330; 100.1455; 100.3020; 110.6770

Key words atmospheric optics; atmospheric turbulence; blind deconvolution; image restoration; telescopes

doi: 10.3788/CJL201239.s209007

1 Instroduction

The resolution of images obtained from the ground-based optical telescopes will be degraded by the atmospheric turbulence. However, it is significantly different for short-exposure images that, whereas atmospheric turbulence severely limits the effective resolution of a long-exposure image that is obtained by an uncompensated, ground-based telescope, short-exposure images retain diffraction-limited information. Since Labeyrie[1] first pointed out this fact, this technique has been extended to other areas. The Knox[2] method and triple correlation[3] recover diffraction-limited information by using the Fourier phase spectra as well as energy spectra, so that the high resolution image can be obtained. All of these techniques require an important condition that a reference unresolved star must be available nearby the object. For this reason, the blind deconvolution techniques proposed by Ayers *et al*.[4] at first are applied to recover the atmospheric blurred images with the atmospheric turbulence point spread function (PSF) unknown. They used an interactive algorithm and enforced a positivity constraint as well as a support constraint. Davey *et al*.[5] improved this technique and decreased the noise further. Form the mathematical view, the convergence properties of blind deconvolution algorithm have been proved by Lane *et al*.[6,7] and the conjugate gradient blind deconvolution was proposed. Jefferies *et al*.[8] developed the conjugate gradient blind deconvolution technique, and applied blind deconvolution technique to remove the atmospheric turbulence blur in real extended object images. Thiebaut *et al*.[9] discussed the algorithm constraints specially. There is an important idea and development in these techniques that is to use a series of short-exposure images of the object, as Schulz[10] first suggested, and it is called multi-frame blind deconvolution. The use of multi-frame short exposure images makes the convergence properties of blind deconvolution algorithm further increase, and decreases the noise in restoration images at the same time.

There are many wide field-of-view (FOV) images obtained by telescopes that the FOV is greater than the isoplanatic angle in the real astronomical observation. The restoration images will be of low quality, where these images are reconstructed by the speckle imaging or blind deconvolution techniques based on the space-invariant imaging formation. Adaptive optics corrects the wavefront error introduced by atmospheric turbulence at the case of anisoplanatic FOV with several guide stars, but the effectiveness of correction images is not perfect[11,12]. The atmospheric PSF is space-variant function when the FOV of the telescope is greater than the isoplanatic angle. The relationship of the atmospheric imaging will not be a simple convolution of the object and PSF. The PSF will be space-variant. Some researchers consider making the image into small sub-regions, and within the sub-region image the PSF is space-invariant so that the blind deconvolution techniques can recover the atmospheric turbulence blurred images[13]. The restored sub-region images are split jointed together. But there is some ringing at edges in the split joint image, and the resolution of the split joint image is low[14,15]. Gonsalves *et al*.[16,17] used the phase diversity technique to recover the wide FOV solar ima-

ges with the sub-region image method. The sub-region image blind deconvolution technique is widely used in other fields, including the adaptive optics image, space satellite image and space to ground object image[15,18~22].

In this paper, we describe our conjugate gradient blind deconvolution algorithm for the astronomical object with unknown PSF, including the improved constraints condition, the band limited, noise filter. To test the algorithm, a series of short-exposure images are produced based on simulating atmospheric turbulence phase screen and PSF. The subject of recovering anisoplanatic extended astronomical object images is investigated, including images split, ringing at image edges and image split joint. Finally, the results of restoration images from real Saturn data are given.

2 Atmospheric turbulence image formation

Due to atmospheric turbulence, the objects $o(\boldsymbol{x})$ are recorded by digital CCD on the ground-based telescope and the resolution of the recorded image $d(\boldsymbol{x})$ is seriously lower. Under the conditions of the isoplanatic FOV, the telescope imaging is approximated as linear space invariant. The performance of the imaging system (atmosphere and telescope) is represented by a space invariant PSF $s(\boldsymbol{x})$. The atmospheric turbulence image formation is

$$d(\boldsymbol{x}) = o(\boldsymbol{x}) * s(\boldsymbol{x}) + n(\boldsymbol{x}), \tag{1}$$

where $n(\boldsymbol{x})$ is the noise considered as Gaussian type. In Eq.(1), the image recorded by telescope is a product of object convolution PSF under the isoplanatic condition. The optical wavefront distortion due to atmospheric turbulence is the major factor affecting the image resolution. In enough short time, the wavefront distortion is approximated as invariable so that a thin random phase screen on the aperture of telescope is used to represent the wavefront distortion. The phase screen can be generated by power spectrum method, given by

$$W(\boldsymbol{x}) = C\iint_{\infty} R(\boldsymbol{k})\ \sqrt{F_{\phi}(\boldsymbol{k})}\exp(\mathrm{j}\boldsymbol{x}\cdot\boldsymbol{k})\mathrm{d}\boldsymbol{k}, \tag{2}$$

$$F_{\phi}(\boldsymbol{k}) = 0.490 r_0^{-5/3}(k^2 + k_0^2)^{-11/6}, \tag{3}$$

where r_0 is the atmospheric coherent length, $\boldsymbol{k}$ is the wave vector, $R(\boldsymbol{k})$ means the complex Gauss random process with the zero mean and unit variance, C is a the constant, k_0 is 0.5, and $F_{\phi}(\boldsymbol{k})$ presents the phase fluctuation power spectrum with Kolmogorov statistical distribution. The system PSF corresponding to short-exposure image is given by

$$s(\boldsymbol{x}) = \left| F^{-1}\left\{ P(\boldsymbol{u})\exp\left[\mathrm{j}\frac{2\pi}{\lambda}W(\boldsymbol{u})\right]\right\}\right|^2, \tag{4}$$

where $P(\boldsymbol{u})$ is the pupil function, whose diameter can determine the system's diffraction limit. The object's short-exposure image can be generated by true object image convolution PSF:

$$i(\boldsymbol{x}) = o(\boldsymbol{x}) * s(\boldsymbol{x}). \tag{5}$$

Figure 1 shows the true object image, the simulated PSF image and the short-exposure image, where the atmospheric coherent length is 10 cm.

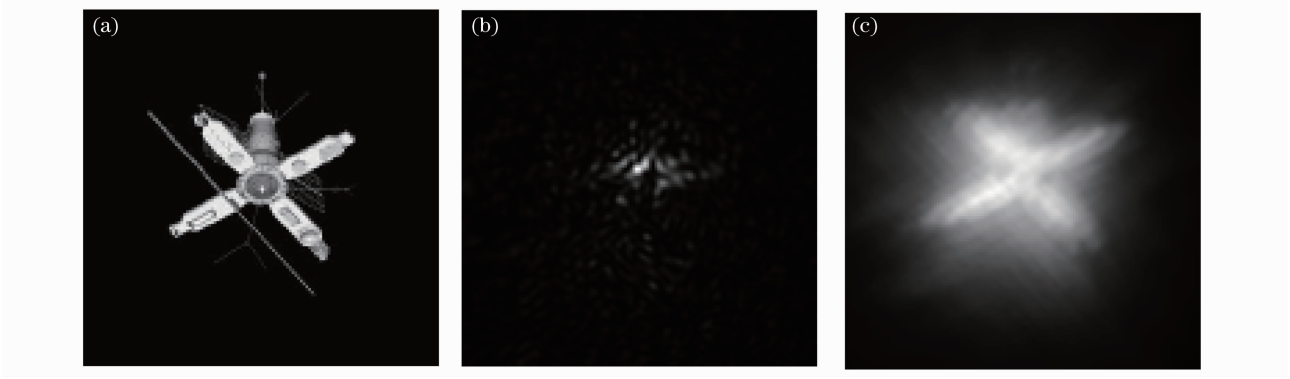

Fig. 1. Simulated short-exposure image of space object. (a) True object image; (b) PSF image; (c) short-exposure image

3 Conjugate gradient blind deconvolution algorithm

From the atmospheric imaging equation [Eq.(1)], to solve the object function, the information about PSF, recorded image and noise data is needed. But, in many cases, the PSF and noise are unknown for astronomical observation. According to the least-squares rule, we start from the initial estimate of the true object $\hat{o}(\boldsymbol{x})$ and PSF $\hat{s}(\boldsymbol{x})$, make the difference between the recorded image $d(\boldsymbol{x})$ and the convolution image $\hat{o}(\boldsymbol{x}) * \hat{s}(\boldsymbol{x})$ minimized by using step by step iteration, and finally reach to obtain the true object image. The cost function is given by

$$\boldsymbol{J} = \sum_k \sum_i [d_k(\boldsymbol{x}_i) - \hat{s}_k(\boldsymbol{x}_i) * \hat{o}(\boldsymbol{x}_i)]^2 + \sum_k \sum_i w_s |\hat{S}_k(\boldsymbol{u}_i)|^2, \tag{6}$$

where $\sum_k \sum_i w_s |\hat{S}_k(\boldsymbol{u}_i)|^2$ considers the constraint of the band limited and noise, so super-resolution in restoration images can be reached, w_s is a smooth widow function. The cost function $\boldsymbol{J}$ is minimized by conjugate gradient optimization approach, with respect to $o(\boldsymbol{x})$ and $s(\boldsymbol{x})$:

$$\frac{\partial \boldsymbol{J}}{\partial o(\boldsymbol{x}_i)} = -2\sum_k \sum_i [d_k(\boldsymbol{x}_i) - \hat{s}_k(\boldsymbol{x}_i) * \hat{o}(\boldsymbol{x}_i)] * \hat{s}_k^+(\boldsymbol{x}_i), \tag{7}$$

$$\frac{\partial \boldsymbol{J}}{\partial s_k(\boldsymbol{x}_i)} = -2\sum_k \sum_i [d_k(\boldsymbol{x}_i) - \hat{s}_k(\boldsymbol{x}_i) * \hat{o}(x_i)] * \hat{o}^+(\boldsymbol{x}_i) + \frac{2}{N^2} w_s \hat{S}_k(\boldsymbol{u}) \sum_{u=0}^{N-1} \left\{ \frac{\partial \hat{S}_k(\boldsymbol{u})}{\partial \mathrm{Re}\, S_k(\boldsymbol{u})} + \mathrm{j} \frac{\partial \hat{S}_k(\boldsymbol{u})}{\partial \mathrm{Im}\, S_k(\boldsymbol{u})} \right\} \exp\left(\mathrm{j}2\pi \frac{ux}{N}\right). \tag{8}$$

During the cost function minimization, the pixel values of object image and PSF image are continuously modified pixel by pixel through the iteration. This iteration is given by

$$\hat{o}^{\mathrm{new}}(\boldsymbol{x}_i) = \hat{o}^{\mathrm{old}}(\boldsymbol{x}_i) + \alpha \frac{\partial J}{\partial o(\boldsymbol{x}_i)}, \tag{9}$$

$$\hat{s}_k^{\mathrm{new}}(\boldsymbol{x}_i) = \hat{s}_k^{\mathrm{old}}(\boldsymbol{x}_i) + \alpha \frac{\partial J}{\partial s_k(\boldsymbol{x}_i)}, \tag{10}$$

where α is the convergence parameter determined by $\{\hat{o}, \hat{s}\} = \arg\min_{\alpha} \boldsymbol{J}$. The important constraints, such as the positivity, unit power and band limit deduced by real telescope system parameters, as well as multiple image frames, are considered in the algorithm iteration. The initial object image $\hat{o}^0(\boldsymbol{x})$ is produced by using several recorded image add, and the initial PSF $\hat{s}^0(\boldsymbol{x})$ is simulated from Eq. (4).

Figure 2 shows the is results of restoration image by the blind deconvolution algorithm from the simulated short-exposure images of space object, where five short-exposure images are applied, the signal-to-noise ratio (SNR) is 30 dB, and the atmospheric turbulence is $r_0 = 10$ cm.

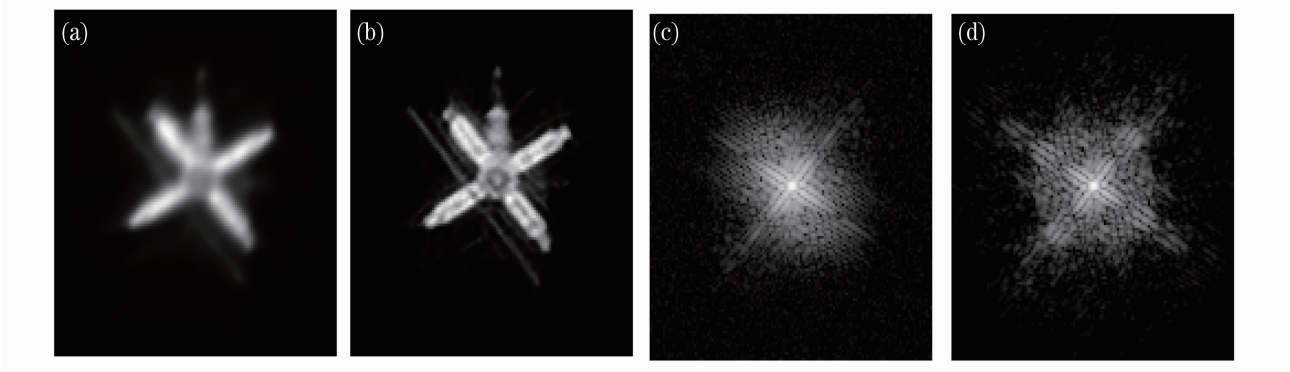

Fig. 2. Restoration images from short-exposure images by blind deconvolution algorithm. (a) Simulated short-exposure image; (b) restoration image; (c); (d) power spectrum images

4 Anisoplanatic image processing

Anisoplanatism happens in the images obtained by telescope when the system FOV is greater than ioplanatic angle, and the PSF becomes space variant. After the anisoplanatic image is preprocessed, it can be recovered by the above blind deconvolution approach. The image is partitioned into small sub-regions corresponding to the space invariant PSF, each sub-region image is processed by blind deconvolution algorithm, and the results are then sewn together to obtain the restored image. Due to the sudden pixel at the edge of the sub-region image, there will be high frequency value at the Fourier power spectrum, and serious ringing will happen in the restored image. To avoid ringing at the edges of restored image, a window function, which has the pixel value reduced to zero smoothly, is designed. The window function is

$$T(m,n) = 1 - \left[\frac{(m,n) - N/2}{N/2}\right]^2. \tag{11}$$

Figure 3 is image of the window function. Simulation experiments show that the proposed window function is more effective than Hanning window to reduce the ringing of restored image.

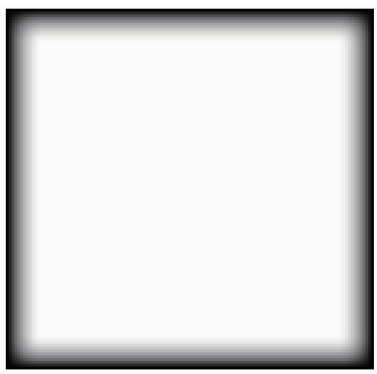

Fig. 3. Image of the widow function

Figure 4 shows the is result of the restoration image by blind deconvolution algorithm for the windowed image. The raw data are the solar image coming from Swedish Vacuum Space Telescope (SVST) with the size of 128 pixel × 128 pixel. Figure 4(a) is the result without the window. Figure 4(b) is the restoration image with the window, there is little ringing in the image.

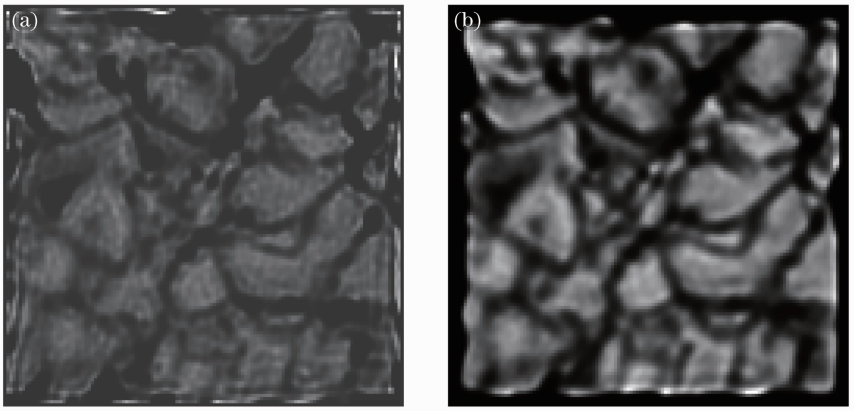

Fig. 4. Effect of window functron on image restoration. (a) Without window; (b) with window

To reduce the sub-region image at the edges, larger overlapping regions are used, and the location coordinate of sub-region image need be remembered. After sewing together sub-region images, the trail at the split line can be removed through the data smoothing manner.

5 Real astronomical image experiments

We use a set of real data to test our blind deconvolution algorithm. The raw data were obtained from the ground-based optical telescope of Yunnan Astronomical Observatory, Chinese Academy of Sciences. Figure 5 is the Saturn short-exposure image. The exposure time was 10 ms, and the size was 1024 pixel × 1024 pixel. The whole image was partitioned into the 12 sub-regions, each 256 pixel × 256 pixel. Figure 6 shows two sub-region short-exposure images [Figs. 6(a), (b)] and their restoration images [Figs. 6(c), (d)]. From the restored sub-region images, we can see that the resolution of the images is improved, and the ringing at the edges is not obvious. Figure 6(e) is the estimated PSF by the blind decovolution algorithm from the sub-region shorts exposure image.

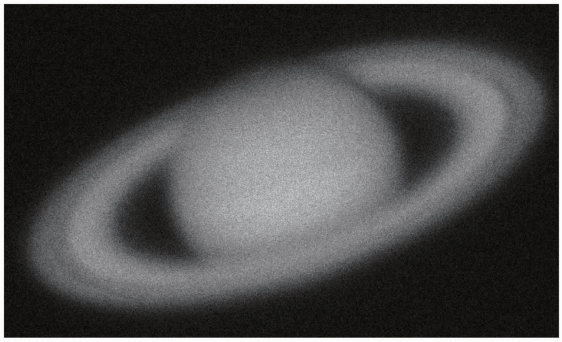

Fig. 5. Saturn short-exposure image

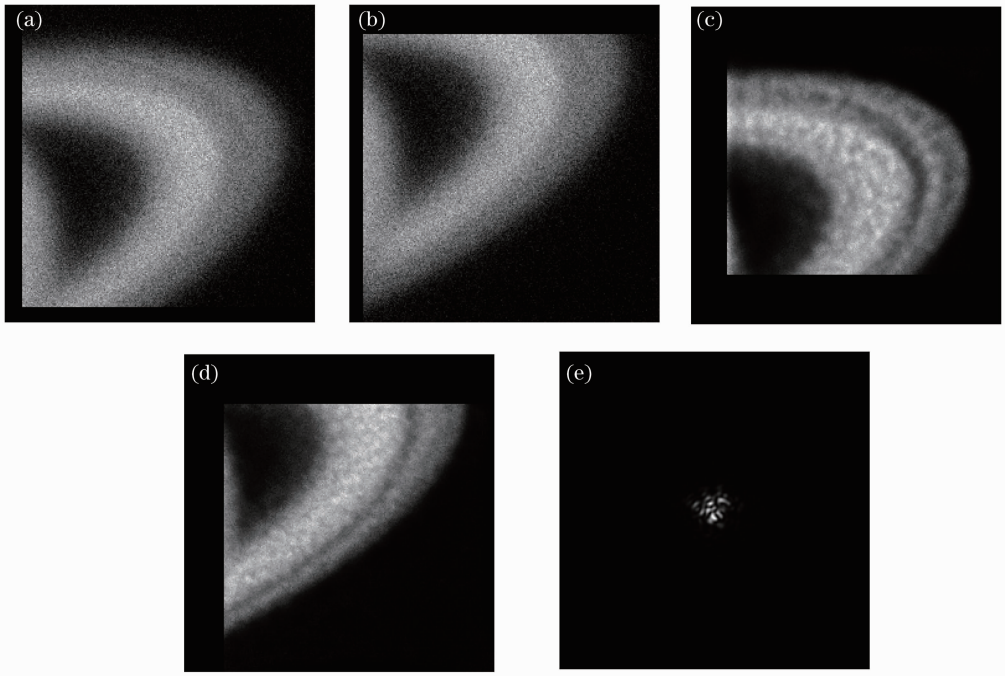

Fig. 6. Results of sub-region restoration image by blind deconvolution; (a), (b) sub-region short-exposure images; (c), (d) restoration images; (e) estimated PSF

Figure 7 is the result of the restored sub-region images sewn together by the blind deconvolution algorithm. The restored image shows that our approach can obtain better image resolution by recovering from the anisoplanatic image degraded by atmospheric turbulence.

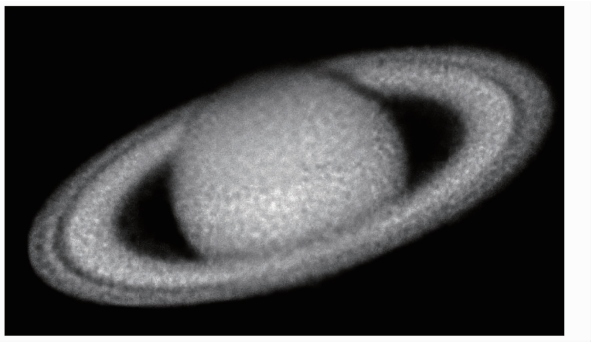

Fig. 7. Saturn restoration image of the restored sub-region images sewn together

6 Conclusion

We describe the atmospheric imaging formation through the ground-based optical telescope. To test our blind deconvolution algorithm, a series of space object short-exposure images are simulated with the space variant PSF, which is generated by a random phase screen. The conjugate gradient blind deconvolution algorithm is presented based on the least-squares approach. Some improved constraints are used to enhance the algorithm convergence. The simulation results illustrate that the proposed blind deconvolution algorithm can obtain high resolution and reduce the noise from the image degraded by atmospheric turbulence. We then investigate the approach for recovering anisoplanatic image degraded by atmospheric turbulence. To apply the blind deconvolution, the anisoplanatic images are partitioned into small sub-region images, and a window function is used to smooth the edge to avoid the ringing in the image. The restored sub-region images are sewn together. Finally, an experimental result of real Saturn image degraded by atmospheric turbulence is presented, and the restoration image shows that the blind deconvolution algorithm is effective to recover anisoplanatic images.

7 Acknowledgement

This work was supported by the National High Technology Research and Development Program (863 Program) of China (2010AA00405) and the Southwest Jiaotong University Science Fund (X1200812430235).

References

1 A. Labeyrie. Attainment of diffraction-limited resolution in large telescope by Fourier-analyzing speckle patters in star images [J]. *Astron. Astrophys.*, 1970, **6**(1): 85～87

2 K. T. Knox, B. J. Thompson. Recovery of images from atmospherically degraded short-exposure photographs [J]. *Astrophys. J. Lett.*, 1974, **193**(1): 45～48

3 A. Lohmann, G. Weigelt, B. Wirnitzer. Speckle masking in astronomy: triple correlation theory and applications [J]. *Appl. Opt.*, 1983, **22**(24): 4028～4037

4 G. R. Ayers, J. C. Dainty. Iterative blind deconvolution method and its applications [J]. *Opt. Lett.*, 1988, **13**(7): 547～549

5 B. L. K. Davey, R. G. Lane, R. H. T. Bates. Blind deconvolution of noisy complex-valued image [J]. *Opt. Commun.*, 1989, **69**(5): 353～356

6 R. G. Lane, R. H. T. Bates. Automatic multidimensional deconvolution [J]. *J. Opt. Soc. Am. A*, 1987, **4**(1): 180～188

7 R. G. Lane. Blind deconvolution of speckle images [J]. *J. Opt. Soc. Am. A*, 1992, **9**(9): 1508～1514

8 S. M. Jefferies, J. C. Christou. Restoration of astronomical images by iterative blind deconvolution [J]. *Astrophys. J.*, 1993, **415**(2): 862～874

9 E. Thiebaut, J. M. Conan. Strict *a priori* constraints for maximum-likelihood blind deconvolution [J]. *J. Opt. Soc. Am. A*, 1995, **12**(3): 485～492

10 T. J. Schulz. Multiframe blind deconvolution of astronomical images [J]. *J. Opt. Soc. Am. A*, 1993, **10**(5): 1064～1073

11 M. I. Charnotskii. Anisoplanatic short-exposure imaging in turbulence [J]. *J. Opt. Soc. Am. A*, 1993, **10**(3): 492～501

12 G. Cresci, R. I. Davies, A. J. Baker *et al*.. Accounting for the anisoplanatic point spread function in deep wide-field adaptive optics images [J]. *Astron. Astrophys.*, 2005, **438**(2): 757～767

13 H. Trussell, B. Hunt. Image restoration of space-variant blurs by sectioned methods [J]. *IEEE Trans. Acoust., Speech, Signal Process*, 1978, **26**(6): 608～609

14 A. F. Boden, D. C. Redding, R. J. hanisch *et al*.. Massively parallel spatially variant maximum-likelihood restoration of Hubble Space Telescope imagery [J]. *J. Opt. Soc. Am. A*, 1996, **13**(7): 1537～1545

15 M. Aubailly, M. Roggemann, T. J. Schulz *et al*.. Approach for reconstructing anisoplanatic adaptive optics images [J]. *Appl. Opt.*, 2007, **46**(24): 6055～6063

16 Robert A. Gonsalves. Nonisoplanatic imaging by phase diversity [J]. *Opt. Lett.*, 1994, **19**(7): 493～495

17 Richard G. Paxman, Brian J. Thelen, John H. Seldin. Phase-diversity correction of turbulence-induced space-variant blur [J]. *Opt. Lett.*, 1994, **9**(6): 1231～1233

18 Nasreddine Hajlaoui, Caroline Chaux, Guillaume Perrin *et al*.. Satellite image restoration in the context of a spatially varying point spread function [J]. *J. Opt. Soc. Am. A*, 2010, **27**(6): 1473～1481

19 Jose M. Bioucas-Dias, Mario A. T. Figueiredo, Joao P. Olivei. Total variation-based image deconvolution a majorization-minimization approach [C]. Proceedings of IEEE International Conference on Acoustics, Acoustics, Speech and Signal Processing, 2006, **2**: 861～864

20 M. A. Vorontsov, G. W. Carhart. Anisoplanatic imaging through turbulent media: image recovery by local information fusion from a set of short-exposure images [J]. *J. Opt. Soc. Am. A*, 2001, **18**(6): 1312～1324

21 Mikhail Charnotskii. Superresolution in dewarped anisoplanatic images [J]. *Appl. Opt.*, 2008, **47**(28): 5110～5116

22 J. Bardsley, S. Jefferies, J. Nagy *et al*.. A computational method for the restoration of images with an unknown, spatially-varying blur [J]. *Opt. Express*, 2006, **14**(5): 1767～1782

栏目编辑：李文喆